Journal of Thermal Analysis and Calorimetry, Vol. 97 (2009) 1, 11–18

THE EFFECT OF K^+ ION EXCHANGE ON THE STRUCTURE AND THERMAL REDUCTION OF HEXAGONAL AMMONIUM TUNGSTEN BRONZE

I. M. Szilágyi[1*], *J. Madarász*[2], *G. Pokol*[2], *F. Hange*[3], *G. Szalontai*[4], *Katalin Varga-Josepovits*[5] *and A. L. Tóth*[6]

[1]Materials Structure and Modeling Research Group of the Hungarian Academy of Sciences, Budapest University of Technology and Economics, 1111 Budapest, Szt. Gellért tér 4, Hungary
[2]Department of Inorganic and Analytical Chemistry, Budapest University of Technology and Economics, 1111 Budapest, Szt. Gellért tér 4, Hungary
[3]GE Hungary ZRt., GE Consumer and Industrial – Lighting, 1340 Budapest, Váci út 77, Hungary
[4]NMR Laboratory, University of Pannonia, 8200 Veszprém, Egyetem u. 10, Hungary
[5]Research Institute for Technical Physics and Materials Science, Hungarian Academy of Sciences, 1121 Budapest, Konkoly-Thege út 29–33, Budapest, Hungary
[6]Department of Atomic Physics, Budapest University of Technology and Economics, 1111 Budapest, Budafoki út 8, Hungary

This paper discusses the changes in the structure and thermal reduction of nanosize hexagonal ammonium tungsten bronze (HATB), $(NH_4)_{0.33-x}WO_{3-y}$, which were caused by K^+ ion exchange (doping) and studied by XRD, XPS, ^{1}H-MAS NMR, FTIR, SEM and TG/DTA-MS. Comparison of the cell parameters of undoped and doped HATB revealed that both *a* and *c* cell parameters decreased after the ion exchange reaction, which showed that smaller K^+ ions partly replaced the larger NH_4^+ ions in the hexagonal channels of HATB. After the reaction, from the hexagonal channels less NH_3 evolved, which also supported the incorporation of K^+ ions into the hexagonal channels.

Keywords: *^{1}H-MAS NMR, hexagonal ammonium tungsten bronze, ion exchange, reduction, SEM, TG/DTA-MS, XPS, XRD*

Introduction

Tungsten oxides and tungsten bronzes are widely studied and used in catalysis [1–3], photoelectrochemical cells [4, 5], secondary batteries [6], chromogenic (electro- [7–9], photo- [10], gaso- [11] and thermochromic [12]) devices and gas sensors [13, 14]. Hexagonal ammonium tungsten bronze (HATB), $(NH_4)_{0.33-x}WO_{3-y}$, owing to its unique properties, is a particularly interesting member of tungsten oxides and tungsten bronzes. It has mixed conductivity, i.e. it can conduct both protons (because of H^+ containing species such as NH_3, NH_4^+, H_2O, OH-group) and electrons (because of e-hopping between W^{6+}, W^{5+} and W^{4+} atoms) [15]. It has an open-tunneling structure and ability to exchange its NH_4^+ ions with metallic cations [16–19].

The ion exchange property of HATB has several application potentials, e.g. in nuclear waste treatment, in non-sag tungsten production, in secondary batteries, etc. In recent studies about using tungsten bronzes in nuclear waste treatment, it was reported that radioactive Cs^+ and Sr^+ were adsorbed successfully by hexagonal sodium tungsten bronzes [20, 21]. Hexagonal ammonium tungsten bronze might be an even better candidate in this field because of its better ion exchange characteristics. In the powder metallurgical production of tungsten lamp filaments, HATB is already one of the most important compounds that may be intermediates. Partial reduction of the starting material, ammonium paratungstate tetrahydrate (APT), $(NH_4)_{10}[H_2W_{12}O_{42}]\cdot 4H_2O$ between 400 and 600°C produces an intermediate product (called 'tungsten blue oxide'), a possible mixture of different phases. It is doped with K, Al and Si, which ensure – after a complete reduction in hydrogen – an overlapping crystallite structure of tungsten powder, which finally provides an appropriate mechanical stability (a so-called 'non-sag' feature) to tungsten filaments even at high operating temperatures in lamps [22–24]. Among the possible constituents of 'tungsten blue oxide' (X-ray amorphous phase, WO_3, $WO_{2.9}$, $WO_{2.72}$, WO_2, tungsten bronzes [16, 17, 22, 23, 25], HATB) may have a special role in tungsten production, because during the doping process through ion exchange reactions it can form ionic bonds with K^+, which ion is the most vital dopant for tungsten lamp filaments [16–19].

Though the ion exchange property of HATB plays a significant role for many application fields and particularly for the production of tungsten powder for lamp industry, there is little knowledge

* Author for correspondence: imre.szilagyi@mail.bme.hu

1388–6150/$20.00

Akadémiai Kiadó, Budapest, Hungary
Springer, Dordrecht, The Netherlands

about the exact chemical mechanism of ion exchange. The structure of hexagonal tungsten bronzes is built up by corner-sharing WO_6 octahedra, which form three- and six-sided channels. The hexagonal channels are partly filled with alkaline ions; in the case of HATB with NH_4^+ ions and NH_3 molecules [22]. It was known that some kind of ion exhange reaction occurs if alkaline ion containing solutions were added to HATB [16–19] or to other hexagonal tungsten bronzes [20, 21], but it was unknown where these alkaline ions get bonded exactly, i.e. whether they are adsorbed only at the surface of the bronze particles or they can also build into the hexagonal channels of the crystalline structure.

Therefore we intended to answer this question and find experimental proof for the possible incorporation of alkaline ions into the hexagonal channels of HATB during the ion exchange reactions (Fig. 1). HATB can be prepared by several ways (e.g. by thermal annealing of ammonium polytungstates, as well as by hydrothermal [15, 26] and solvothermal [27, 28] synthesis methods), but now the partial reduction of APT is the only way, by which highly crystalline HATB can be produced. Recently we studied the thermal decomposition of APT in detail [29–31]. A model was proposed on the formation of HATB through the annealing of APT, and on the basis of this model monophase, highly ordered nanosize HATB sample could be prepared [32]. This allowed us to study the incorporation of alkaline ions into HATB.

In this study we aimed to explore the ion exchange reaction between HATB and K^+ ion. For this we applied the standard doping reaction used in the production of tungsten powder for lamp industry [23, 24], i.e. KCl and $AlSiO_3$ solutions were added to HATB. To investigate the changes in the structure, composition and morphology caused by doping with K^+, we studied HATB before and after the doping reaction with X-ray diffraction (XRD), X-ray photoelectron spectroscopy (XPS), solid state ^{1}H-MAS (magic angle spinning), NMR spectroscopy, FTIR spectroscopy and scanning electron microscopy (SEM). XRD was selected to detect the possible change in the crystalline structure of HATB due to the incorporation of K^+ ions. XPS was used to detect K^+ on the surface of the particles, and through depth profiling also inside the particles. With ^{1}H-MAS NMR the change in the concentration of proton containing species (NH_4^+, NH_3, H_2O, OH-group) was supposed to be studied. FTIR was aimed to investigate the alteration of bonds and the change in the concentration of NH_3 and NH_4^+ due to ion exchange. Morphology changes were supposed to be detected by SEM.

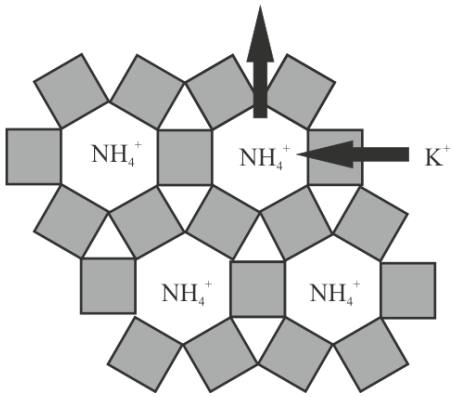

Fig. 1 Substitution of NH_4^+ at the hexagonal channels of HATB with K^+ ions

The doping usually also causes changes in the reduction course of tungsten oxides and tungsten bronzes [23, 33, 34], and to explore such changes the thermal reduction of HATB and doped HATB was studied with XRD, simultaneous TG/DTA and evolved gas analysis (TG/DTA-MS). The literature about the thermal reduction of undoped [18] and doped [35] HATB was rather lacking. However, recently we managed to detect three different positions of NH_4^+ ions and NH_3 molecules in HATB with TG/DTA and evolved gas analysis [36]. Therefore it was expected that thermal analysis should be a valuable analytical method to decide that NH_4^+ ions at which positions have been involved in the ion exchange reaction with K^+.

Experimental

Highly ordered, monophase nanosize hexagonal ammonium tungsten bronze, HATB, $(NH_4)_{0.07}(NH_3)_{0.04}(H_2O)_{0.09}WO_{2.95}$ was prepared by heating ammonium paratungstate tetrahydrate (APT), $(NH_4)_{10}[H_2W_{12}O_{42}]\cdot 4H_2O$ in H_2 for 6 h at 400°C [32]. Intermediate solid products of HATB were prepared in a Setaram TG/DTA 92 thermal analyzer in 10% H_2/Ar (75 mL min^{-1}, open platinum crucible, 10°C min^{-1} heating rate, m_0=80–100 mg). Doped HATB was produced by adding KCl and $AlSiO_3$ solutions to HATB.

During the evolved gas analytical (TG/DTA-MS) measurements open platinum crucible, sample sizes of ~150 mg, a heating rate of 10°C min^{-1} and flowing 10% H_2/He (130 mL min^{-1}) were used for purging the thermoanalytical furnace. The TG/DTA-MS apparatus consisted of an STD 2960 Simultaneous DTA/TG (TA Instruments Inc.) thermal analyzer and a Thermostar GSD 200 (Balzers Instruments) quadrupole mass spectrometer. On-line coupling between the two parts was provided through

a heated (T=200°C) 100% methyl deactivated fused silica capillary tube with inner diameter of 0.15 mm. A mass range between m/z=1–64 was monitored through 64 channels in multiple ion detection mode (MID) with a measuring time of 0.5 s/channel. The components of released gaseous mixtures were monitored and identified on the basis of their MS reference gas spectra [37].

Powder X-ray diffraction (XRD) patterns were recorded by a PANalytical X'pert Pro MPD X-ray diffractometer equipped with an X'Celerator detector using CuK_α radiation. For cell parameter determination of HATB and doped HATB, Si (ICDD 27-1402) was applied as an internal standard, and deconvolution of peaks, baseline correction, splitting of peaks from $CuK_{\alpha1}$ and $K_{\alpha2}$ radiation as well as for profile fitting were conducted.

Scanning electron microscopy (SEM) characterization was performed by a LEO-1550 FEG SEM instrument.

X-ray Photoelectron Spectroscopy (XPS) spectra were collected by a VG Microtech instrument consisting of a XR3E2 X-ray source, a twin anode (MgK_α and AlK_α) and a CLAM 2 hemispherical analyser using MgK_α radiation. Detailed scans were recorded with 50 eV pass energy at (0.05 eV/1.5 s). The spectrometer was calibrated with the binding energy of the C 1s line (284.5 eV).

Solid state ^{1}H-MAS (magic angle spinning) NMR experiments were carried out on a Varian Unity 300 spectrometer supplied with Doty XC5 solid phase ^{1}H head at 4000 Hz rotor spinning frequency in an XC5 insert (special sample holder), which was set inside a Si_3N_4 rotor. ^{1}H chemical shifts were referenced to TMS (δ_{1H}=0 ppm).

FTIR spectra were measured between 400–4000 cm^{-1} by an Excalibur Series FTS 3000 (Biorad) FTIR spectrophotometer in KBr pellets.

Results and discussion

Characterization of HATB

XRD analysis showed that the HATB sample was highly crystalline and contained only the hexagonal ammonium tungsten bronze phase, which was identified by ICDD 42-0452 card in space group $P6_3/mcm$, No. 193 [32].

According to SEM images, HATB was built up by 50–100 nm nanograins, which were aggregated into micrometer scale particles (Fig. 2). Therefore HATB preserved the micro-morphology of its precursor, APT, which consisted of μm scale particles, but the nano-morphology changed a great deal, when 50–100 nm HATB particles were formed as HATB crystallized during the annealing of APT [36].

After refining the XPS spectrum belonging to HATB sample (Fig. 3), W^{4+} ($W4f_{7/2}$=34.7 eV and $W4f_{5/2}$=32.8 eV) and W^{5+} ($W4f_{7/2}$=36.0 eV and $W4f_{5/2}$=33.7 eV) atoms were also observed besides W^{6+} ($W4f_{7/2}$=37.1 eV and $W4f_{5/2}$=35.0 eV) atoms. Furthermore, NH_3 molecules (N1s=399.7 eV) were detected also besides NH_4^+ ions (N1s=401.9 eV) [32].

In the ^{1}H-MAS NMR spectrum of HATB (Fig. 3a), the large peak around 5 ppm seemed to be asymmetric, and could be fitted properly only with

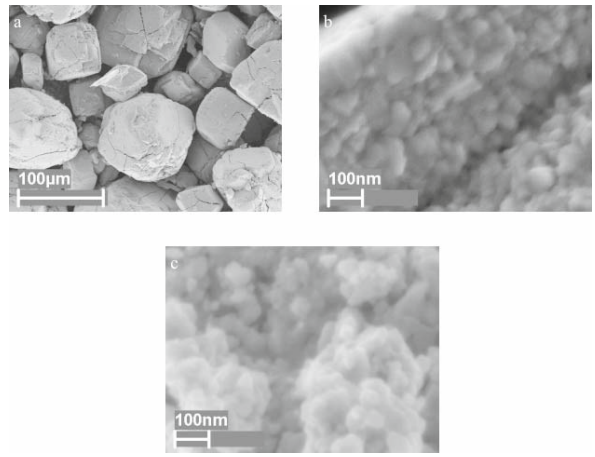

Fig. 2 SEM image of a–b – HATB and c – doped HATB

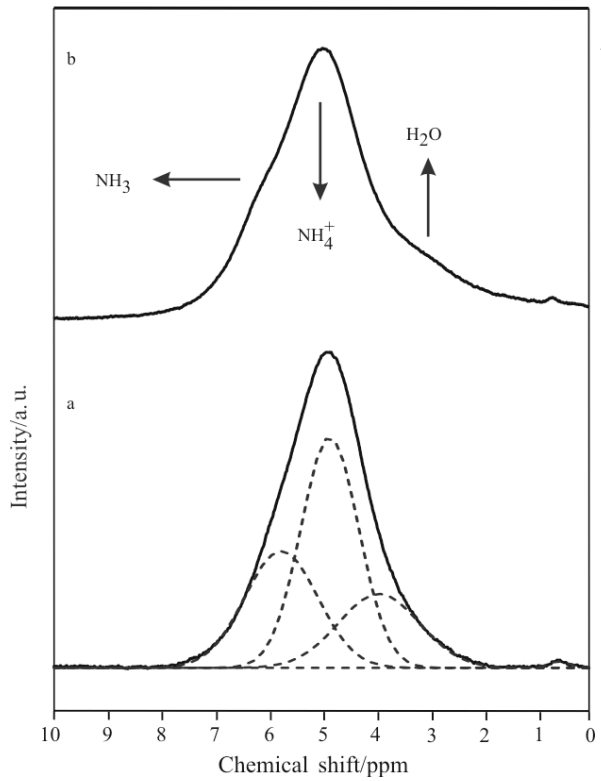

Fig. 3 ^{1}H-MAS NMR pattern of a – HATB and b – doped HATB

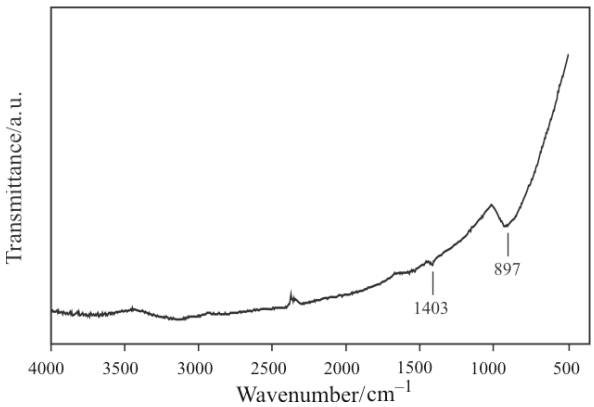

Fig. 4 FTIR spectrum of HATB

hree peaks. The peak at 4.9 ppm was assigned to NH_4^+ ions. The peak at 5.8 ppm was supposed to belong to NH_3 molecules, whose presence was already detected by XPS. The peak at 4.0 ppm was assumed to come from water molecules bounded on the surface of or inside the bronze particles [32].

In the infrared spectrum of HATB (Fig. 4) a broad peak was observed at 897 cm^{-1}, accompanied by a shoulder at 700–750 cm^{-1}, which were assigned to W–O vibrations [15, 38]. The 0.83 mass/mass% NH_4^+ ion and NH_3 molecule content [32] was represented by a small peak of N–H deformation vibration at 1403 cm^{-1} and by a broad, low intensity peak of N–H stretching vibration over 3000 cm^{-1}. This latter region referred also to water molecules and OH-groups bounded on/in the particles. The negative peak around 2300 cm^{-1} was due to the varying CO_2 content of the optical path.

The composition of HATB sample was determined by combining the results of various techniques (XPS, ^{1}H-MAS NMR, TG, titration) and $(NH_4)_{0.07}(NH_3)_{0.04}(H_2O)_{0.09}WO_{2.95}$ was obtained for the formula of HATB sample [32].

The effect of K^+ ion exchange on the structure of HATB

After the ion exchange reaction, the crystalline structure remained the same and no new reflections were observed compared to the XRD pattern of HATB before doping. If K^+ ion builds into the crystalline structure of HATB, then this may cause changes in cell parameters. To investigate this 4-4 XRD measurements were conducted both on HATB and doped HATB (Table 1). The results showed that both *a* and *c* cell parameters decreased after the ion exchange reaction, and two explanations were considered for this. The first option was that K^+ ions did not build into the structure. Thus, the decrease of cell parameters was caused only by the release of NH_4^+ and NH_3 from the hexagonal channels, and by the contraction of the emptied hexagonal channels. According to the second explanation, K^+ ions did build into the structure. In this case the decrease of cell parameters can be rationalized by that the smaller K^+ ions (0.133 nm ionic radius [39]) partly replaced the larger NH_4^+ ions (0.143 nm ionic radius [39]) in the hexagonal channels.

Previous experimental results were in agreement with the second explanation. Recently it was shown that if HATB was heated and NH_4^+ and NH_3 left the hexagonal channels, the *a* cell parameter decreased, but the *c* cell parameter increased [40]. The increase of *c* cell parameter can be explained by that less NH_4^+ and NH_3 were in the hexagonal channels and they could not contract electrostatically the hexagonal channels along the *c* axis so much [17]. As a contrast, both *a* and *c* cell parameters decreased after the ion exchange in our experiments. This suggested that in our study the decrease of cell parameters was caused not by the sole release of NH_4^+ and NH_3, but rather by the partial substitution of the larger NH_4^+ ions with smaller K^+ ions in the hexagonal channels.

After the ion exchange reaction, on the surface of particles, W, O and N belonging to HATB were detected with XPS. Si originating from the dopant solutions could be also observed well, but only traces of K were visible in the XPS spectrum and Al was undetectable. In the detailed spectrum of O, the O atoms (533.3 eV) of dopant compounds (preferably silicates) were also identified besides the O atoms of HATB (530.6 eV) [41]. These results show that dopant compounds adsorbed on the surface of HATB particles during doping. We tried to check if K had been present in traces not only on the surface of but also inside the HATB particles. For this the surface of doped HATB was sputtered with Ar^+ ions (15 min,

Table 1 Cell parameters of HATB and doped HATB

HATB			Doped HATB		
No.	*a*/nm	*c*/nm	No.	*a*/nm	*c*/nm
1	0.73841	0.75394	4	0.73816	0.75378
2	0.73863	0.75379	3	0.73835	0.75360
3	0.73830	0.75390	1	0.73810	0.75395
4	0.73839	0.75374	2	0.73824	0.75342
Mean	0.73843	0.75384	Mean	0.73824	0.75367

0.5 μA). Recently W_2O_3 thin films were prepared with atomic layer deposition (ALD) [42] and their composition was studied with XPS. There XPS combined with sputtering was a very effective analytical tool, since a few nm deep WO_3 film covered the sample, which could be sputtered away with Ar^+ ions, and then the composition of the bulk film (W_2O_3) could be determined easily. As a contrast, here in this study Ar^+ ion sputtering distorted the crystalline structure so much that due to oxygen loss even $W^{(0)}$ species ($W4f_{7/2}$=32.5 eV and $W4f_{5/2}$=30.5 eV) appeared [32]. After sputtering only traces of N were observed, and K could not be detected at all. Since sputtering distorted the structure, it is highly probable, that even if K had been built into the particles, with XPS it could not have been detected.

In the ^{1}H-MAS NMR spectrum of doped HATB (Fig. 4b), large shoulders appeared on both sides of the peak belonging to NH_4^+ ions (5 ppm). The increase of the peak of NH_3 molecules (6 ppm) compared to the peak of NH_4^+ ions shows that the ratio of NH_3 molecules increased compared to NH_4^+ ions. Since NH_3 molecules do not have electric charge, they do not tend to take part in the ion exchange reaction with K^+. Therefore after the doping reaction the overall amount of NH_4^+ ions was expected to decrease compared to NH_3. With ^{1}H-MAS NMR it was not yet possible to make distinction between NH_4^+ ions on the surface of and inside the particles but at least it was clearly shown that some kind of ion exchange had occurred. In addition, after doping the amount of H_2O molecules (4.0 ppm) also increased compared to NH_4^+, which can be explained by that HATB could adsorb a great deal of H_2O from the doping solutions.

In the FTIR spectrum only minor changes occurred after doping. We could not observe significant reduction of the band at 1403 cm^{-1}. This showed that the sensitivity of FTIR was not enough to detect the amount of NH_4^+ that left HATB due to the ion exchange with K^+. During the doping process also new bonds were formed, but these changes were below the detection limit of this technique.

According to SEM investigation, no significant changes in the morphology of HATB were observed after doping (Fig. 2).

Thermal reduction of HATB

The simultaneous TG, DTG and DTA curves of the thermal reduction of HATB are presented in Fig. 5. Seven decomposition steps were observed up to 900°C, which are marked on the DTG curve. With evolved gas analysis the evolution of H_2O and NH_3 was detected (Fig. 6).

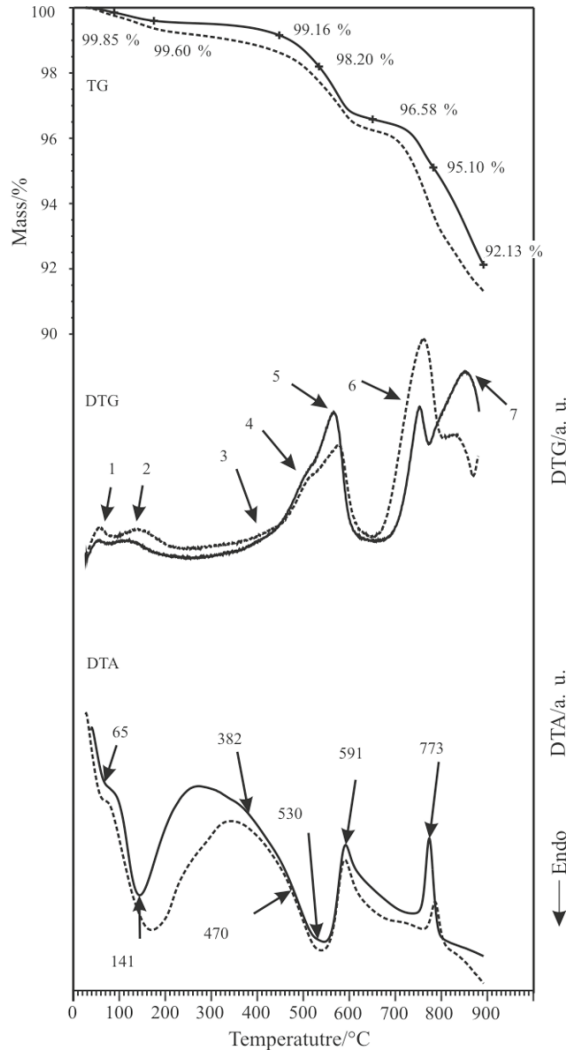

Fig. 5 Simultaneous TG/DTG/DTA curves of — – HATB and --- – doped HATB measured in 10% H_2/He (130 mL min^{-1}, 10°C min^{-1}, open Pt crucible, 150.9 and 152.1 mg respectively)

Up to 250°C absorbed and chemisorbed H_2O evolved in two overlapping endothermic reactions (DTG curve, peaks 1–2). From 250–650°C water and ammonia were released in three overlapping steps (DTG curve, peaks 3–5, 250–450°C, 450–500°C, 500–650°C). The release of NH_3 molecules in three consecutive steps was explained by that NH_3 molecules (which originated from the NH_4^+ and NH_3 content of HATB [36]) came from three different positions of HATB particles, where they were bonded with different strength. In the first step they came from the surface of the particles, in the second step either from a second surface position or from the disordered space between crystallites and in the third step from the hexagonal channels of the crystallites. We discussed recently the detection of different

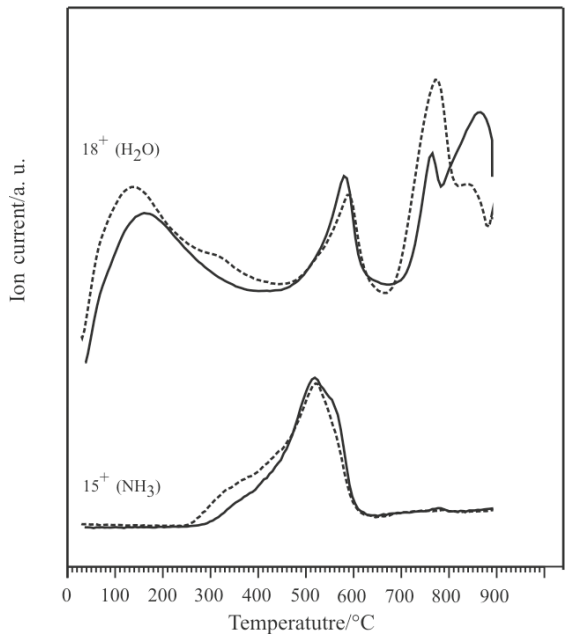

Fig. 6 Ion current curves of gaseous species evolved from — – HATB and --- – doped HATB measured by on-line coupled TG/DTA-MS system in 10% H_2/Ar (130 mL min^{-1}, 10°C min^{-1}, open Pt crucible, 150.9 and 152.1 mg respectively)

cation positions in HATB in detail [36], and more explanations were considered for the origin of NH_3, which evolved in three different steps. On the basis of theoretical considerations and experimental results, the explanation above was found to be the most probable.

Despite the continuous release of NH_3 and H_2O, the structure of HATB did not change (Fig. 7). The major difference between HATB and the decomposition intermediate at 550°C was that the hexagonal channels became almost completely empty at 550°C (shown indirectly by TG/DTA-MS). Therefore to indicate this change and to be consistent with the literature, this phase was called reduced h-WO_3.

Then between 550–650°C the hexagonal structure collapsed, when most of the stabilizing NH_3 molecules and NH_4^+ ions were purged out of the hexagonal channels (the stabilizing effect of these species is discussed elsewhere [36]). Since here the metastable reduced h-WO_3 transformed into a more stable compound, this reaction was exothermic, and it changed the DTA curve into exothermic. Recently it was found that in oxidative and inert atmospheres the hexagonal WO_3 structure collapsed in an exothermic reaction also, but there h-WO_3 transformed into monoclinic (m-) WO_3 [36]. Here, in reductive atmosphere the hexagonal structure was highly reduced, and this oxygen lacking environment blocked the formation of m-WO_3. Instead, another ammonium tungsten bronze phase (β-HATB),

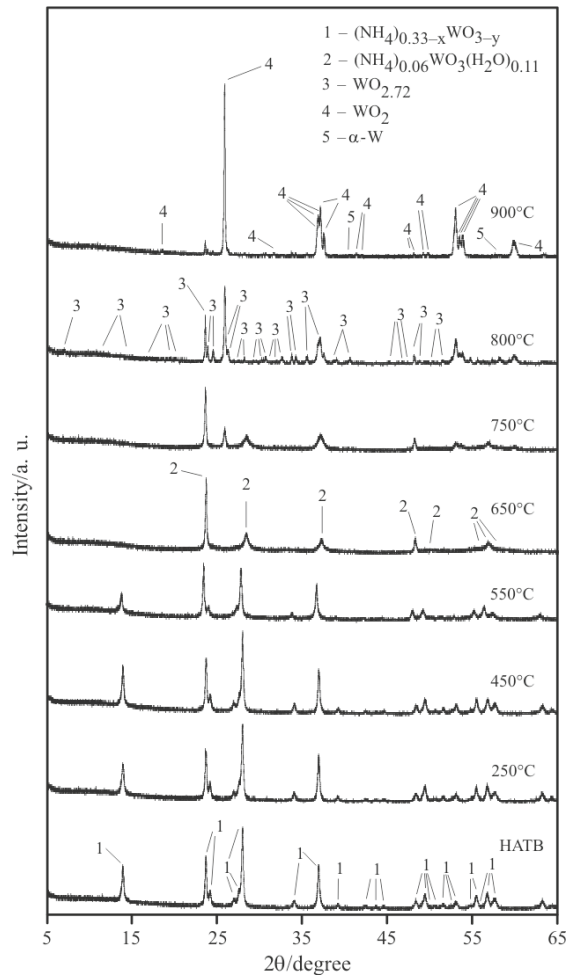

Fig. 7 XRD patterns of intermediate solid products of HATB decomposed in 10% H_2/Ar

$(NH_4)_{0.001}WO_{2.79}$ with small ammonium ion content formed in a pure form. The structure and composition of β-HATB is discussed elsewhere [42].

Between 650–800°C H_2O and small amounts of NH_3 were released and β-HATB decomposed into γ-tungsten oxide, $WO_{2.72}/W_{18}O_{49}$ (ICDD 05-0392, 36-0102) and δ-tungsten oxide, WO_2 (ICDD 32-1393). The exothermic DTA peak 750–800°C was assigned to the formation and crystallization heat of $WO_{2.72}/W_{18}O_{49}$ [42].

Finally in the seventh decomposition step (from 800°C) H_2O was released as reduction product of tungsten oxides without any sharp heat effect. The intermediate at 900°C consisted of WO_2 with traces of α-tungsten, W (ICDD 04-0806) and $WO_{2.72}/W_{18}O_{49}$.

The effect of K^+ ion exchange on the thermal reduction of HATB

There was only one study about the thermal reduction of doped HATB, where Mészáros *et al.* studied the

evolution of NH_3 from undoped and doped HATB between 400–600°C with EGA-MS, and they mentioned that doping with K^+ changed the NH_3 evolution curves [35], but they gave no explanation for this. Our study was expected to bring more information about the thermal reduction of doped HATB, and explain the changes in the NH_3 evolution curves, because more complex and more sensitive analytical techniques were used.

The simultaneous TG, DTG and DTA curves of the reduction of doped HATB are presented in Fig. 5, the evolved gas analytical curves are shown in Fig 6. Here only those features of the curves are discussed, which differed from the thermoanalytical curves before doping.

In the first (25–100°C) and second (100–250°C) decomposition steps the amount of released water increased, which can be rationalized by that HATB could adsorb and chemisorb more water from the doping solution than from air. In the third step (250–450°C) the amount of evolved NH_3 increased, in the fourth step (450–500°C) no significant change was observed, while in the fifth step (500–650°C) the amount of released NH_3 decreased, which is similar to the observations of Mészáros *et al.* [35]. These observations mean that after the ion exchange with K^+, the amount of NH_3 and NH_4^+ on the surface of particles increased, while their amount decreased in the hexagonal channels.

According to the XRD study, both *a* and *c* cell parameters of HATB decreased after doping, which suggested that K^+ ions had substituted partially NH_4^+ ions in the hexagonal channels. Therefore less NH_3 was expected to be released from the hexagonal channels between 500–650°C, which corroborates our TG/DTA-MS measurements. The NH_4^+ ions leaving the hexagonal channels had to move to such position where they were bonded weaker (preferably onto the surface of particles), and this can explain the increased amount of released NH_3 between 250–450°C. So the TG/DTA-MS study also supported that K^+ ions partly replaced NH_4^+ ions in the hexagonal channels of HATB.

The thermoanalytical curves above 650°C also showed some changes, which can be explained by that doping usually cause changes in the reduction course of tungsten oxides and tungsten bronzes [23, 33, 34].

Conclusions

In this paper the changes in the structure and thermal reduction of nanosize hexagonal ammonium tungsten bronze (HATB), $(NH_4)_{0.07}(NH_3)_{0.04}(H_2O)_{0.09}WO_{2.95}$, caused by K^+ ion doping were studied with XRD, XPS, ^{1}H-MAS NMR, FTIR, SEM and TG/DTA-MS. The goal was to decide that during the doping process whether K^+ was also incorporated in the hexagonal channels of HATB or it just adsorbed only on the surface of the particles.

With XPS Si and traces of K were detected on the surface of doped HATB, which showed that dopant compounds adsorbed on the surface of HATB particles during doping. Since Ar^+ ion sputtering distorted the structure too much, depth profiling of K was not successful. With ^{1}H-MAS NMR it was observed, that the amount of NH_4^+ decreased in HATB after doping, which supported that the ion exchange reaction between NH_4^+ and K^+ really took place. XRD analysis showed that doping did not change the overall structure of HATB. However, comparison of the cell parameters of undoped and doped HATB revealed, that both *a* and *c* cell parameters decreased after doping, which indirectly suggested that K^+ was built into the hexagonal channels of HATB, since the ionic radius of K^+ is smaller than that of NH_4^+.

The study on the thermal reduction of undoped and doped HATB also supported that K^+ ions partially replaced NH_4^+ ions not only on the surface of HATB particles, but also in the hexagonal channels of the crystallites. Before doping, NH_3 was released in three consecutive, overlapping steps, which was explained by that NH_3 and NH_4^+ were bonded at three different positions in HATB, i.e. (*i*) on the surface of particles, (*ii*) on a second kind of surface position or between crystallites and (*iii*) in the hexagonal channels. The hexagonal framework collapsed and transformed into another ammonium tungsten bronze (β-HATB) when most of the stabilizing NH_3 molecules and NH_4^+ ions were purged out of HATB. From β-HATB reduced tungsten oxides ($WO_{2.72}$/$W_{18}O_{49}$ and WO_2) and finally tungsten metal (α-W) formed. After doping the formation of reduced tungsten oxides was affected to some extent above 650°C. The main difference in the thermal reduction of doped HATB compared to undoped HATB was that from the surface of doped HATB particles more NH_3 evolved and the amount of NH_3 released from the hexagonal channels decreased (the as-released NH_3 originated from both the NH_3 and NH_4^+ content of HATB). This suggested that K^+ ions partly substituted NH_4^+ ions in the hexagonal channels and due to this the amount of NH_4^+ ions reduced in the hexagonal channels. NH_4^+ ions leaving the hexagonal channels moved onto the surface of particles, and this increased the amount of NH_3 released from the surface of HATB.

Acknowledgements

I. M. S. thanks for an Aschner Lipót scholarship of GE Hungary ZRt., GE Consumer and Industrial – Lighting. A diffractometer purchase grant from the Agency for Research Fund Management and Research Exploitation (KPI-EU-GVOP-3.2.1.-2004-04-0224/3.0 KMA) is gratefully acknowledged.

References

1 R. Gao, X. Yang, W. L. Dai, Y. Le, H. Li and K. Fan, J. Catal., 256 (2008) 259.
2 C. F. Lin, C. H. Wu and Z. N. Onn, J. Hazard. Mater., 154 (2008) 1033.
3 T. Arai, M. Yanagida, Y. Konishi, Y. Iwasaki, H. Sugihara and K. Sayama, Catal. Commun., 9 (2008) 1254.
4 S. Higashimoto, T. Shishido, Y. Ohno, M. Azuma, M. Takahashi and M. Anpo, J. Electrochem. Soc., 154 (2007) F48.
5 C. Santato, M. Odziemkowski, M. Ulmann and J. Augustynski, J. Am. Chem. Soc., 123 (2001) 10639.
6 A. C. Dillon, A. H. Mahan, R. Deshpande, P. A. Parilla, K. M. Jones and S. H. Lee, Thin Solid Films, 518 (2008) 794.
7 S. F. Hong and K. C. Chen, Electrochim. Acta, 53 (2008) 5306.
8 S. R. Bathe and P. S. Patil, Solid State Ionics, 179 (2008) 314.
9 S. Sallard, T. Brezesinski and B. M. Smarsly, J. Phys. Chem., C 111 (2007) 7200.
10 Y. He, Z. Wu, L. Fu, C. Li, Y. Miao, L. Cao, H. Fan and B. Zou, Chem. Mater., 15 (2003) 4039.
11 H. Chen, N. Xu, S. Deng, D. Lu, Z. Li, J. Zhou and J. Chen, Nanotechnology, 18 (2007) 205701.
12 S. M. A. Durrani, E. E. Khawaja, M. A. Salim, M. F. Al-Kuhaili and A. M. Al-Shukri, Sol. Energy Mater. Sol. Cells, 71 (2002) 313.
13 C. Balázsi, K. Sedlacková, E. Llobet and R. Ionescu, Sens. Actuators B, 133 (2008) 151.
14 S. J. Kim, P. S. Cho, J. H. Lee, C. Y. Kang, J. S. Kim and S. J. Yoon, Ceram. Int., 34 (2008) 827.
15 L. Huao, H. Zhao, F. Mauvy, S. Fourcade, C. Labrugere, M. Pouchard and J.-C. Grenier, Solid State Sci., 6 (2004) 679.
16 H.-J. Lunk, B. Ziemer, M. Salmen and D. Heidemann, Int. J. Refract. Met. Hard Mater., 12 (1993–1994) 17.
17 H.-J. Lunk, M. Salmen and D. Heidemann, Int. J. Refract. Met. Hard Mater., 16 (1998) 23.
18 B. A. Kiss, G. Rom Berendné, G. Gyarmathy and Z. Kutasi Feketéné, Magyar Kémiai Folyóirat (in Hungarian), 93 (1987) 97.
19 L. Bartha, G. Gyarmati, B. A. Kiss, T. Németh, A. Salamon and T. Szalay, Acta Chim. Acad. Sci. Hung., 101 (1979) 127.
20 C. Luca, C. S. Griffith, E. Drabarek and H. Chronis, J. Nucl. Mater., 358 (2006) 139.
21 C. S. Griffith and V. Luca, Chem. Mater., 16 (2004) 4992.
22 E. Lassner and W.-D. Schubert, Tungsten. Properties, Chemistry, Technology of the Element, Alloys, and Chemical Compounds, Kluwer Academic/Plenum Publishers, New York 1999.
23 L. Bartha, E. Lassner, W.-D. Schubert and B. Lux (Eds), Special Issue on the Chemistry of Non-Sag Tungsten, Int. J. Refract. Met. Hard Mater., 13 (1995) 1.
24 E. Pink and L. Bartha, The Metallurgy of Doped/Non-Sag Tunsgten, Elsevier, London 1989.
25 J. W. van Put and T. W. Zegers, Int. J. Refract. Met. Hard Mater., 10 (1991) 115.
26 T. E. Gier, D. C. Pease, A. W. Sleight and T. A. Bither, Inorg. Chem., 7 (1968) 1646.
27 A. Michailovski, F. Krumeich and G. R. Patzke, Chem. Mater., 16 (2004) 1433.
28 J. H. Zhan, X. G. Yang, Y. Xie, B. F. Li, Y. T. Qain and Y. B. Jia, Solid State Ionics, 126 (1999) 373.
29 I. M. Szilágyi, J. Madarász, F. Hange and G. Pokol, J. Therm. Anal. Cal., 88 (2007) 139.
30 I. M. Szilágyi, J. Madarász, F. Hange and G. Pokol, Solid State Ionics, 172 (2004) 583.
31 J. Madarász, I. M. Szilágyi, F. Hange and G. Pokol, J. Anal. Appl. Pyrol., 72 (2004) 197.
32 I. M. Szilágyi, F. Hange, J. Madarász and G. Pokol, Eur. J. Inorg. Chem., 17 (2006) 3413.
33 B. Zeiler, W.-D. Schubert and B. Lux, Int. J. Refract. Met. Hard Mater., 10 (1991) 91.
34 B. Zeiler, W.-D. Schubert and B. Lux, Int. J. Refract. Met. Hard Mater., 12 (1993–1994) 9.
35 M. Mészáros, J. Neugebauer and F. Hange, High Temp. Mater. Processes, 15 (1996) 111.
36 I. M. Szilágyi, J. Madarász, G. Pokol, P. Király, G. Tárkányi, S. Saukko, J. Mizsei, A. L. Tóth, A. Szabó and K. Varga-Josepovits, Chem. Mater., 20 (2008) 4116.
37 NIST Chemistry Webbook Standard Reference Database, No. 69, 2005, June Release, http://webbook.nist.gov/chemistry
38 A. B. Kiss and L. Chudik-Major, Acta Chim. Acad. Sci. Hung., 78 (1973) 237.
39 Arnold Euchen: Zahlenwerte und Funktionen aus Physik, Chemie, Astronomie, Geophysik und Technik, I. Band: Atom- und Molekularphysik, 4. Teile: Krystalle. Springer, Berlin, Göttingen, Heidelberg 1955.
40 I. M. Szilágyi, I. Sajó, P. Király, G. Tárkányi, A. L. Tóth, A. Szabó, K. Varga-Josepovits, J. Madarász and G. Pokol, J. Therm. Anal. Cal., accepted (paper no. 9876).
41 B. Vincent Crist, Handbook of Monochromatic XPS Spectra, Vol. 1, The Elements and Nature Oxides, XPS International, California 1999.
42 C. L. Dezelah IV, O. M. El-Kadri, I. M. Szilágyi, J. M. Campbell, K. Arstila, L. Niinistö and C. H. Winter, J. Am. Chem. Soc., 128 (2006) 9638.

ICTAC 2008

DOI: 10.1007/s10973-008-9752-1